Article

Charge transport in organic semiconducting crystals exhibiting TADF: insight from quantum-chemical calculations

Andrey Yu. Sosorev[1,2]*, Dmitry I. Dominskiy[1,2], Nikita O. Dubinets[1,3]

1. *Enikolopov Institute of Synthetic Polymeric Materials, Russian Academy of Science, Profsoyuznaya 70, Moscow 117393, Russia*
2. *Faculty of Physics and International Laser Center, Lomonosov Moscow State University, Leninskie Gory 1/62, Moscow 119991, Russia*
3. *Photochemistry Center, FSRC Crystallography and Photonics, Russian Academy of Sciences, Novatorov Str. 7A-1, Moscow, 119421, Russia*

**e-mail: sosorev@physics.msu.ru*

Abstract: Luminophores featuring thermally activated delayed fluorescence (TADF luminophores) are the workhorse of the third- and fourth-generation OLEDs. While these compounds had usually been used as dopants embedded in the host, non-doped TADF OLEDs have recently shown significant progress as well reaching the performance comparable to the host-dopant ones. For efficient operation of the non-doped OLEDs, charge transport in neat films and single crystals of TADF luminophores is important; however, this issue was nearly unexplored theoretically. In the current study, we calculated charge mobilities in four TADF single crystals, which have different molecular packing motifs. Specifically, in one of them both donor and acceptor moieties form uniform π-stacks, while in the others donors (acceptors) show alternating lateral shifts along the stacks; the difference in molecular packing results in the difference of transfer integral between the molecules. Reorganization energies differ as well up to four times for the studied crystals. As a result, charge mobilities vary from 0.001 to ~0.3 $cm^2/(V \cdot s)$, the largest being predicted for the crystal of the luminophore consisting of rigid donor and acceptor. We anticipate that the results obtained can be useful for the design of TADF luminophores for non-doped OLEDs, OLETs and other organic light-emitting devices.

Keywords: OLED, charge mobility, DFT, hopping transport, transfer integrals, reorganization energy

 doi:10.20944/preprints202212.0225.v1

1. Introduction

Organic light-emitting diodes (OLEDs) are leaders in commercialization among the organic electronic devices. Their wide application in the displays and lighting panels is based on their high luminance and contrast, flexibility, true black color, relatively inexpensive production, small weight (no metal and no quartz substrate) and size [1-4]. First generation of OLEDs utilized fluorophores and had small EQE because 75% of the electrically generated excitons were lost in non-emissive triplet states. On the contrary, second-generation OLEDs exploited phosphorescent luminophores, in which triplet excitons were harvested, but these devices suffered from poor color purity and smaller luminance. Finally, third- and fourth-generation OLEDs are based on luminophores exhibiting temperature-activated delayed fluorescence (TADF). In these compounds, triplet states are close in energy to the singlet one, allowing thermal fluctuations to perform reversible intersystem crossing re-populating singlet state from the triplet one and enabling delayed fluorescence [5].

TADF luminophores typically consist of donor and acceptor moieties [5]. Accordingly, frontier molecular orbitals of these luminophores are separated: highest occupied molecular orbital (HOMO) is located mainly on the donor moiety(es), while lowest unoccupied molecular orbital (LUMO) is located mainly on the acceptor moiety(es). Moreover, donor and acceptor moieties are usually orthogonal due to steric hindrance preventing their coplanar orientation. All this weakens the overlapping between HOMO and LUMO and hence decreases the energy difference between the singlet and triplet energy levels, which is necessary for efficient TADF. Although TADF luminophores have highly non-planar and asymmetrical structures, they frequently form single crystals, and molecular packing for several of them was recently reported (see, e.g., Refs. [6-10]). However, detailed analysis of the crystal structures and intermolecular interaction in them is lacking.

Usually, TADF luminophores are used as dopants embedded in the amorphous organic semiconducting host. However, recently, non-doped TADF OLEDs, where pristine films of TADF luminophores serve as light-emitting layers, gained attraction due to the ease of manufacturing and better operational stability and reproducibility [5, 11]. Remarkably, external quantum efficiency (EQE) values for reported non-doped TADF OLEDs are lower but already comparable to those of the conventional (host-dopant) ones [5, 11, 12]. In the non-doped OLEDs, the luminophore film needs to maintain transport of holes and electrons, in contrast to the conventional OLEDs where this function is delivered to the host. Thus, theoretical prediction of electron and hole mobilities is important for design of luminophores for non-doped OLEDs. It is natural to start such investigation from the crystal structures obtained from X-Ray data, since the latter can shed light on the molecular packing typical for the compounds studied. However, theoretical studies of charge transport in crystals or amorphous films of TADF luminophores are extremely rare: we are aware of only one such investigation [13]. It is natural to start such investigation from the crystal structures obtained from X-Ray data, since the latter can shed light on the molecular packing typical for the compounds studied. Thus, comparative theoretical study of charge transport in various TADF crystals is important for revealing structure-property relationships and formulating guidelines for design of TADF luminophores for non-doped OLEDs.

Preprints (www.preprints.org) | NOT PEER-REVIEWED | Posted: 13 December 2022 doi:10.20944/preprints202212.0225.v1

In this work, we compare the crystal structures of four TADF luminophores, oTE-DRZ, CPPD, PXZ-XO and TRZ-c-BPXZ, X-Ray data for which were reported earlier. The Hirshfeld analysis and energy framework approaches are applied to unveil the difference in the crystal packing. In the former crystal, columnar packing of the molecules is observed, where donor and acceptor moieties form segregated π-stacks providing overlap of HOMOs (LUMOs). In the three remaining crystals, donor and acceptor moieties are also segregated, but their packing in the stacks is non-homogeneous: they form tightly interacting dimers, while these dimers interact weakly with their neighbors. We calculate transfer integrals and reorganization energies for the compounds studied, and then estimate hole and electron mobilities therein within the hopping model, which is frequently used to estimate charge mobility in organic semiconductors [14-16]. The relationship between the charge mobilities and molecular/crystal structure is discussed, which can facilitate rational design of TADF luminophores for non-doped OLEDs and other light-emitting organic devices.

2. Methods

Crystal structure analysis

Hirshfeld surface analysis and energy framework calculations were performed in CrystalExplorer21.5 software [17] at the B3LYP-D2/6-31 g (d,p) level. Note that, according to Ref. [18] using the D2 dispersion correction scheme in Crystal Explorer is preferable to using D3. For energy framework calculations, a molecular shell with a 3.8Å radius was generated around a central molecule, and the interaction energies (electrostatic, dispersion and total) between the molecular pairs were calculated. The scale factors for benchmarked energies used for the construction of energy models were taken from Ref. [19]. Crystal structures were obtained from the CCDC database: 1905959 [6], 1922220 [7], 2043193 [9] for oTE-DRZ, CPPD, and TRZ-c-BPXZ respectively, crystal data for PXZ-XO was obtained from Ref. [8]; no further geometry optimization was performed.

Charge mobility

To estimate charge mobility within the hopping model, charge transfer rates from a given molecule A to each of its nearest neighbors (e.g. molecule B) were calculated using the Marcus formula [20]:

$$k_{AB} = \frac{2\pi}{\hbar} J_{AB}^{\ 2} \frac{1}{\sqrt{4\pi\lambda kT}} \exp\left(-\frac{(\Delta E - \lambda)^2}{4\lambda kT} \right) \quad (1)$$

where J is the transfer integral describing electronic interaction between the two molecules, λ is the reorganization energy describing the strength of the electron-phonon coupling, $\hbar$ is the reduced Planck constant, k is the Boltzmann constant, T is the absolute temperature, and ΔE is the electron energy difference between the initial and final sites (ΔE=0 if the molecules are similar). Protocol for J and λ calculation is described below. In the case of molecular "dimerization" along some direction, when the molecule A form tightly interacting dimer with molecule B possessing large J_{AB}, but the latter molecule interacts weakly with the next molecule C in this direction via small J_{BC}, we describe effective transfer rate along this direction as $\widetilde{k_{AB}} = \frac{2k_{AB} \cdot k_{BC}}{(k_{AB}+k_{BC})}$. This expression stems from the fact that the transition time from A to C, $t_{AC}=1/k_{AC}$, is

Preprints (www.preprints.org) | NOT PEER-REVIEWED | Posted: 13 December 2022 doi:10.20944/preprints202212.0225.v1

composed of $t_{AB}=1/k_{AB}$ and $t_{BC}=1/k_{BC}$, and effective $\tilde{k}_{AB}=1/(t_{AC}/2)=2/t_{AC}$. Finally, charge mobility was calculated from Eq. (1) using the Einstein–Smoluchowski relation:

$\mu_0 = \frac{eD}{kT} = \frac{e}{6kT}\sum_i k_i r_i^2 p_i$, where D is the charge carrier (polaron) diffusion coefficient, r_i is the distance between the adjacent molecules along the i-th transport direction, and $p_i = \frac{k_i}{\sum_j k_j}$ is the probability of the charge carrier to move in this direction.

As follows from Eq. (1), main parameters of the hopping model are transfer integrals, J, and reorganization energies, λ. The former were calculated using home-written code based on dimer projection method (DIPRO) [21-23]. To estimate this quantity for a pair (dimer) of molecules (monomers) A and B, the wavefunctions of these molecules were approximated by their lowest unoccupied molecular orbitals (LUMOs), φ_A and φ_B. The latter were written in the basis of the dimer molecular orbitals φ_i:

$$J_{AB} = \langle \varphi_A | H | \varphi_B \rangle = \sum_i \sum_j \langle \varphi_A | \varphi_i \rangle \langle \varphi_i | H | \varphi_j \rangle \langle \varphi_j | \varphi_B \rangle \approx \sum_i \langle \varphi_A | \varphi_i \rangle E_i \langle \varphi_i | \varphi_B \rangle \quad (2)$$

where E_i are the energies of φ_i. Projections of monomer LUMOs on dimer orbitals, $\langle \varphi_A | \varphi_i \rangle$ and $\langle \varphi_i | \varphi_B \rangle$, were calculated from the corresponding coefficients in the basis of atomic orbitals. Reorganization energies λ were approximated by their inner part that is typically considered much larger than the outer part [24]. The λ values were calculated according to the 4-point scheme [24]. In this approach, the energies of the molecule in 4 states are required: neutral state in its optimized geometry (N state), neutral state in the optimized geometry of the charged state (N^*), charged state in its optimized geometry (C), and charged state in the geometry of the neutral state (C^*). The energy difference between the former two states, $\lambda_1 = E_N^* - E_N$, describes the energy relaxation of the molecule that have lost the charge carrier, while the energy difference between the latter two states, $\lambda_2 = E_C^* - E_C$, describes the energy relaxation of the molecule that have accepted the charge. Total reorganization energy is:

$$\lambda = \lambda_1 + \lambda_2 = \left(E_N^* - E_N\right) + \left(E_C^* - E_C\right) \quad (3)$$

DFT calculations were performed using B3LYP functional 6-31g* basis set (for obtaining HOMO/LUMO patterns, electrostatic potential distribution and J estimation) and using CAM-B3LYP functional and the same basis set (for λ computation). GAMESS package [25,26] was used to calculate J and λ for isolated molecules, including ONIOM [27] calculations for λ in crystals. For ONIOM calculations, full optimization was performed, and molecules of the molecular shell were calculated using two-level QM/QM2 approach. The high level (DFT) method was used for the researched molecule (in our case, the central molecule) and low level (HF-3C [28]) method for its environment. The data were visualized using Chemcraft [29] and JMol [30] packages.

Preprints (www.preprints.org) | NOT PEER-REVIEWED | Posted: 13 December 2022 doi:10.20944/preprints202212.0225.v1

3. Results and discussion

Molecular properties

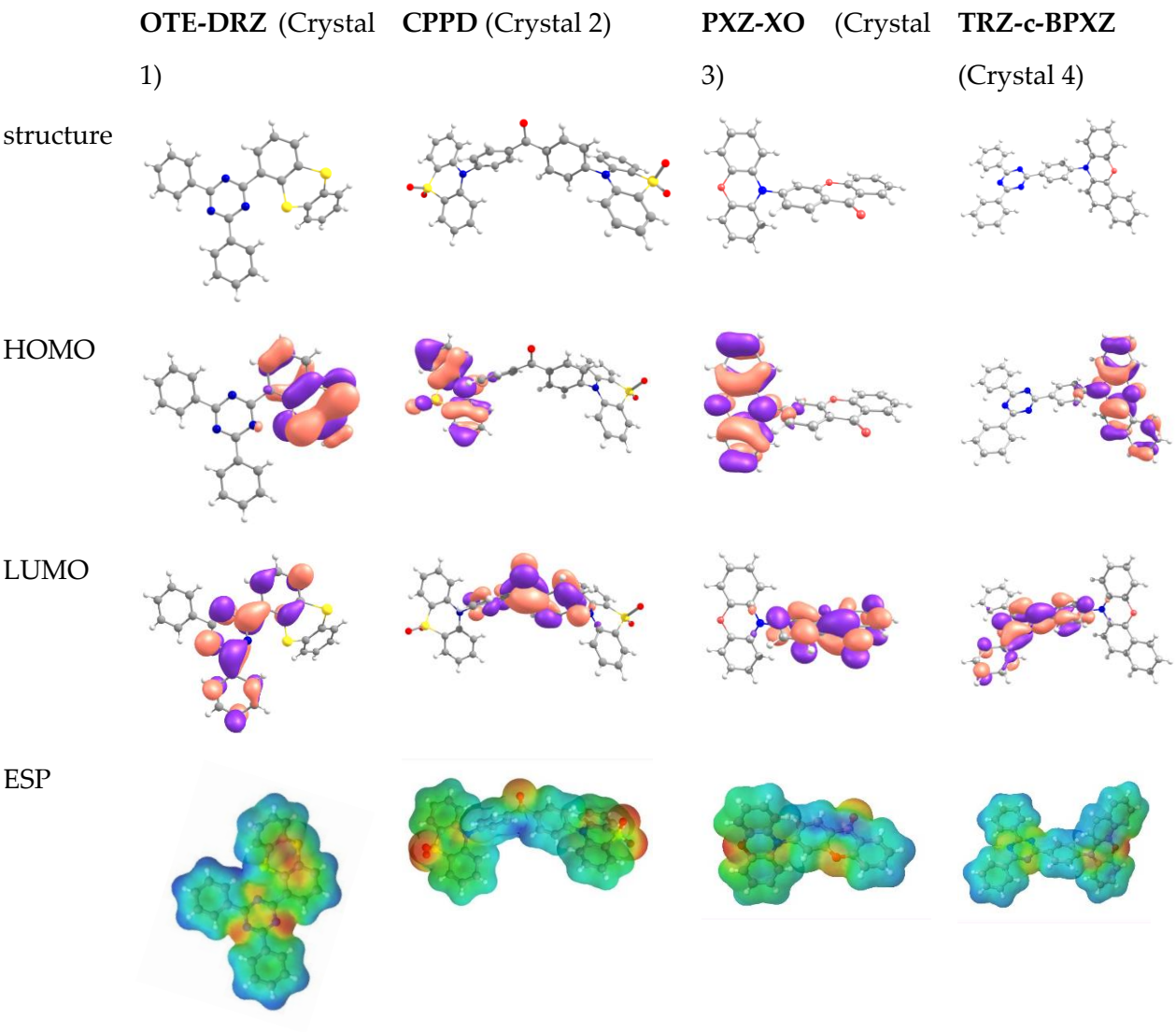

Figure 1. Molecular structures, HOMO and LUMO patterns, and ESP distributions for the compounds studied.

Molecular structures, HOMO and LUMO patterns, and electrostatic potential (ESP) distribution for the molecules constituting the crystals studied are shown in **Figure 1**. All the molecules are asymmetric and non-planar. As expected, HOMOs are located on the donor moieties: 2-(dibenzo-[b,d]thiophen-4-yl) (oTE) in oTE-DRZ, phenothiazine-5,5-dioxide (PTZDO) in CPPD, phenoxazine (PXZ) in PXZ-XO and benzo[a]phenoxazine (BPXZ) in TRZ-BPXZ. LUMOs are located on acceptor moieties: 4,6-diphenyl-1,3,5-triazine (DRZ) in oTE-DRZ (with partial penetration on oTE), benzophenone (BP) in CPPD, 9*H*-xanthen-9-one (XO) in PXZ-XO and 12-(4-(4,6-diphenyl-1,3,5-triazin-2-yl)phenyl) (TRZ) in TRZ-BPXZ. The overlapping of HOMO and LUMO is small, which is a prerequisite for TADF. ESP distribution is non-uniform because of the presence of electronegative atoms (nitrogen and oxygen) in the molecular structure, and asymmetric within both donor and acceptor moieties.

Preprints (www.preprints.org) | NOT PEER-REVIEWED | Posted: 13 December 2022 doi:10.20944/preprints202212.0225.v1

Crystal properties

Figure 2 shows the Hirshfeld surfaces mapped with curvedness for the crystals of studied compounds; the Hirshfeld surfaces mapped with ESP are shown in Figure S1 of the Supporting information (SI). We used curvedness maps to analyze crystal packing and identify planar π-stacking arrangements by relatively large green (i.e., flat) regions [31]. Two of the four studied compounds (oTE-DRZ and PXZ-CMO) crystallize in the triclinic system with the $P\bar{1}$ space group, and other two (CPPD and TRZ-c-BPXZ) in the monoclinic system with the $P2_1/n$ space group, however they do not demonstrate similar packing. Compound oTE-DRZ tends to form one-dimensional stacks (this is clearly seen from the energy framework given in FigureS3a), and the curvedness map in Figure 2a shows one extended green region per each side of the Hirshfeld surface, which indicates that it is a π-stack. It's important to mention, that the π···π contact area between adjacent molecules extends to both donor and acceptor moieties. The second compound CPPD also tends to form one-dimensional stacks (Figure S3b), but since it is centered around twisted benzophenone acceptor part, the π···π contact is very limited (small flat green region in the center of the molecule in Figure 2b). The relatively large green region on the donor part shows how the molecules from adjacent stacks form a dimer with π···π contact. Figure 2c shows how the compound PXZ-XO forms dimers with π···π contacts independently through the donor part and through the acceptor part: only one side of each Hirshfeld surface of donor/acceptor moiety has a large green region. Similar dimerization with π···π contacts is observed for the fourth compound TRZ-BPXZ (Figure 2d), separately for the BPXZ part and for the TRZ part. Yet for both PXZ-XO and TRZ-BPXZ compounds some minor green regions are identified indicating modest π···π contacts with other adjacent molecules. Full list of intermolecular contacts is shown in Figure S2 of SI.

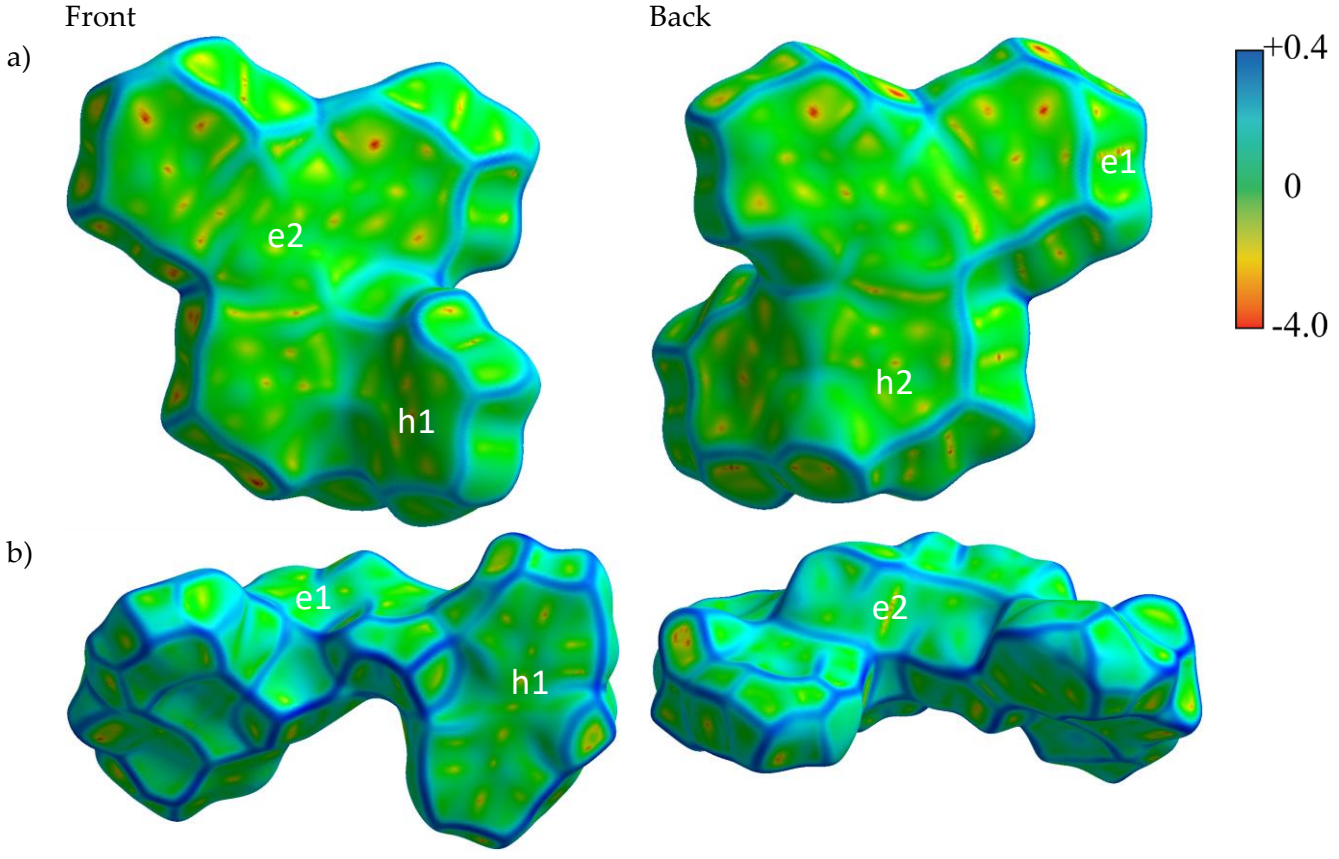

Preprints (www.preprints.org) | NOT PEER-REVIEWED | Posted: 13 December 2022 doi:10.20944/preprints202212.0225.v1

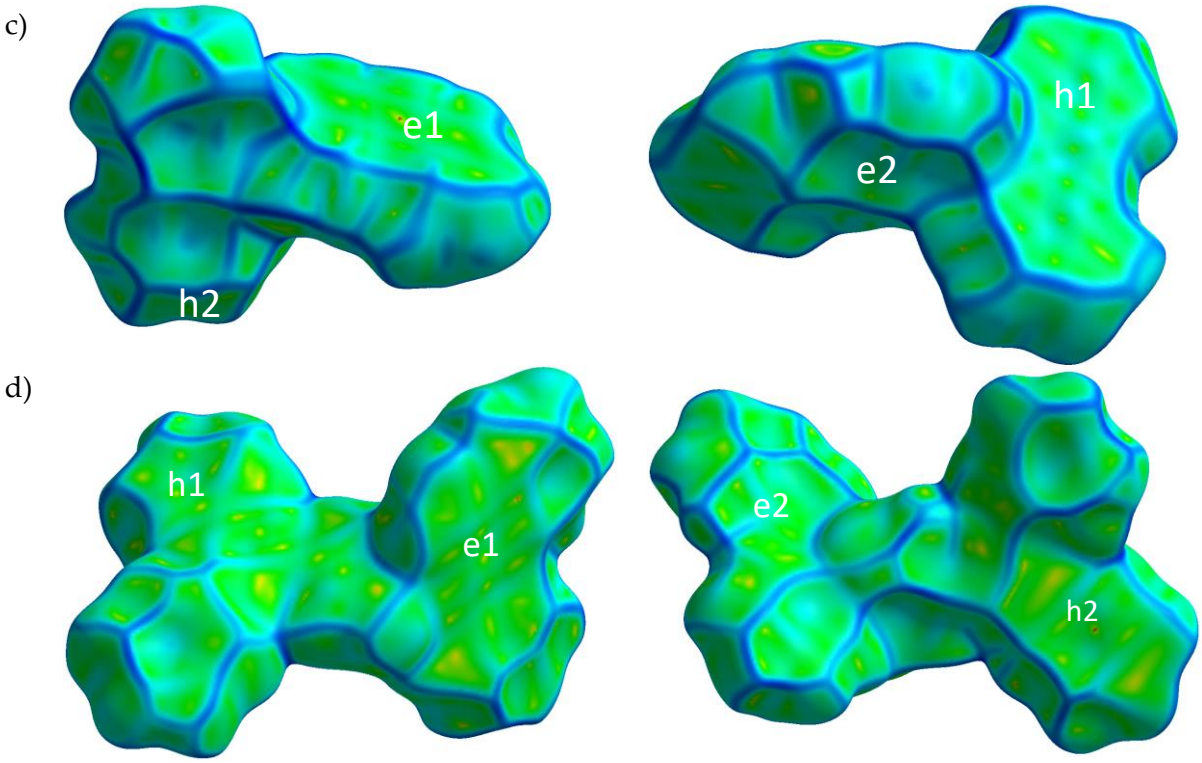

Figure 2. Hirshfeld surfaces (front and back of the molecules) mapped with curvature C [17] for crystalline oTE-DRZ (a), CPPD (b), PXZ-XO (c) and TRZ-c-BPXZ (d). Blue color depicts edges (large curvature), green color depicts relatively flat areas (curvature near unity), and yellow and red depict super flat areas (curvature tends to zero). Labels depict the areas at the surface associated with important contacts for hole ("h") and electron ("e") transport.

Charge transport

Transfer Integrals

Table 1. Hole (J_h) and electron (J_e) transfer integrals for the crystals studied.

Dimer #	J_h, *meV*	J_e, *meV*
oTE-DRZ (Crystal 1)		
1	111	0
2	82	0
3	0	15
4	0	15
5	6	1
6	3	7
7	11	1
8	10	0
CPPD (Crystal 2)		
1	3	0
2	3	0
3	0	94
4	149	0
5	1	26
6	4	0

Preprints (www.preprints.org) | NOT PEER-REVIEWED | Posted: 13 December 2022 doi:10.20944/preprints202212.0225.v1

PXZ-XO (Crystal 3)		
1	23	0
2	5	0
3	3	16
4	47	1
5	0	35
6	1	54
TRZ-c-BPXZ (Crystal 4)		
1	6	2
2	6	2
3	0	12
4	0	172
5	3	1

oTE-DRZ (Crystal 1). Transfer integrals along various directions for all the crystals studied are listed in Table 1. For oTE-DRZ, they are illustrated in **Figure 3a,b**. As mentioned above, this crystal differs from the others since it has a direction where both donor and acceptor moieties form π-stacks. As follows from Figure 3a, large hole transfer integrals exceeding 80 meV are observed in this crystal, which form continuous charge transport path. Figure 3c illustrates that the abovementioned integrals correspond to the π-stacking contacts of the molecules since Hirshfeld surface for them is flat; these contacts also reveal themselves in Figure 2a (areas h1 and h2). Electron transfer integrals are much lower, the largest being 15 meV. As follows from Figure 3d, these integrals are observed for edge-to-edge molecular contacts (area e1 in Figure 2a). Surprisingly, electron transfer integrals are negligible along the π-stack (i.e. for contacts associated with green flat area e2 in Figure 2a), despite of the considerable overlap of the LUMO wavefunctions from the parallel and close-located triazine moieties (Figure S5b). This can be tentatively assigned to the phase mismatch between the two LUMOs in such π-stacking dimers (see Figure S6). Noteworthily, LUMO+1 orbitals of the monomers show J_{LUMO+1}~110 meV for this dimer; the orbital of the dimer composed by LUMO+1 orbitals of monomers (i.e., LUMO+2) lies by ~60 meV above its LUMO, and its population is just ~11 times lower than that of the latter. Thus, this orbital can participate in electron transport, increasing charge mobility in about twice.

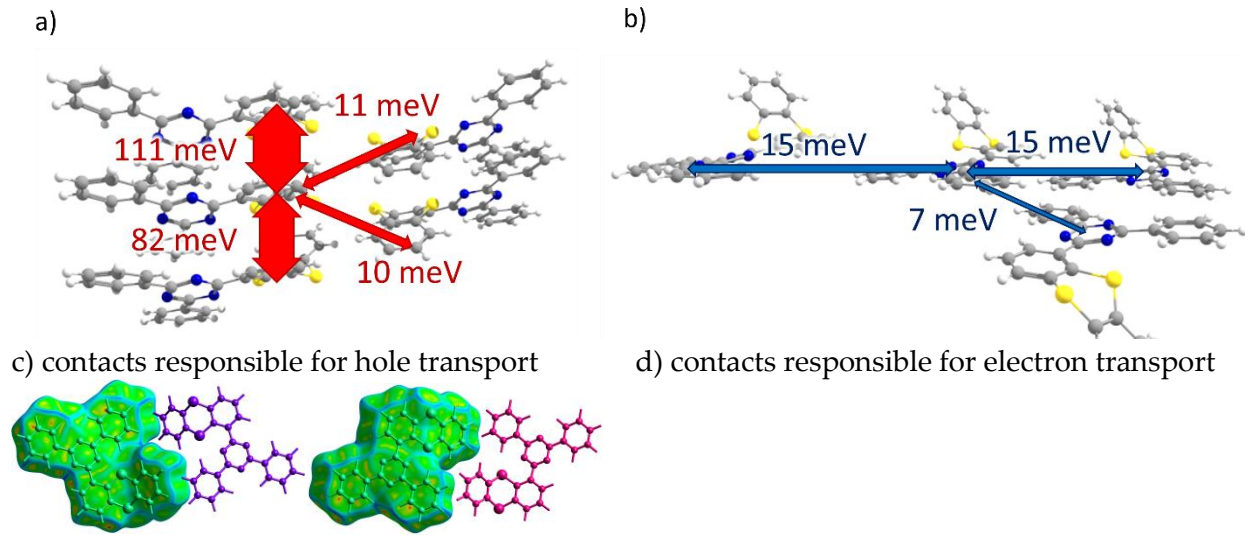

Preprints (www.preprints.org) | NOT PEER-REVIEWED | Posted: 13 December 2022 doi:10.20944/preprints202212.0225.v1

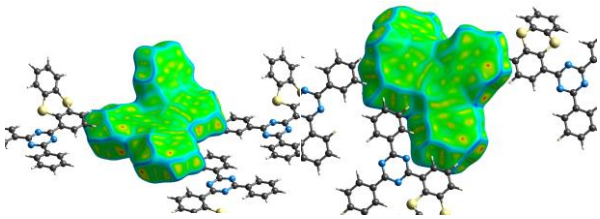

Figure 3. Charge transfer integrals for hole (a) and electron (b) transport in oTE-DRZ. (c,d) Intermolecular contacts enabling these transfer integrals; left and right pictures correspond to different sides of the central molecule. Hirshfeld surface for central molecule is mapped with curvature C. Coloring scale is depicted in Figure 2.

CPPD (Crystal 2). Transfer integrals for CPPD crystal are shown in **Figure 4a,b**. Here, the donor moieties form pairs with large hole transfer integrals (J_h~150 meV), but these dimers are weakly electronically coupled to the donor moieties of the neighboring molecules (all other J_h<5 meV) so that continuous path of considerable J_h is not formed within the crystal. Large J_h are observed for π-stacking contacts revealing themselves as flat green areas in Figure 4c (contact with the molecule colored in blue) and Figure 2b (area h1), where donor moieties lie one above another in an antiparallel manner with small lateral shifts. Acceptor moieties also form tightly bound pairs with J_e=94 meV, and these dimers are coupled to the neighboring ones by moderate J_e=26 meV, so that reasonable electron mobility can be expected for this crystal. Because of the twisted character of BP acceptor moieties, their stacking is less pronounced (see Figure 4d and Figure 2b, areas e1 and e2).

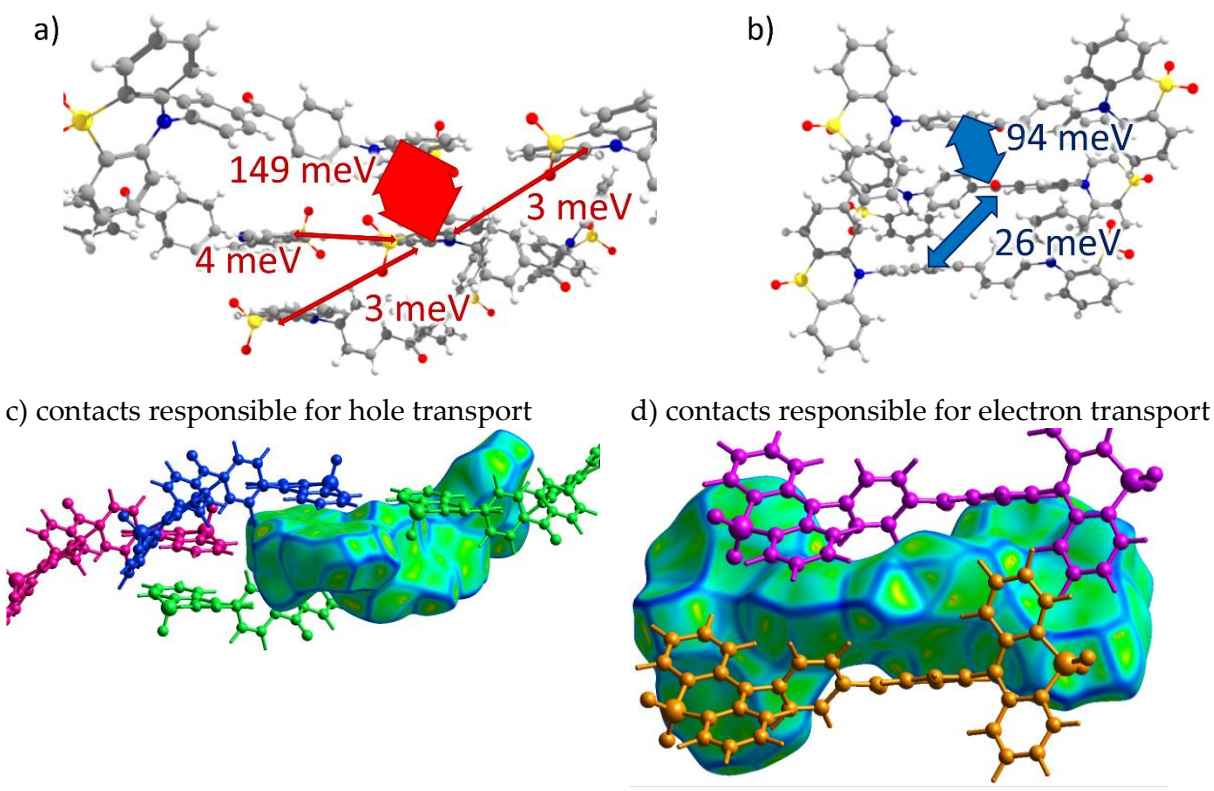

Figure 4. Charge transfer integrals for hole (a) and electron (b) transport in CPPD. (c,d) Intermolecular contacts enabling these transfer integrals; Hirshfeld surface for central molecule is mapped with curvature C. Coloring corresponds to Figure 2.

Preprints (www.preprints.org) | NOT PEER-REVIEWED | Posted: 13 December 2022 doi:10.20944/preprints202212.0225.v1

PXZ-XO (Crystal 3). **Figure 5**a,b shows transfer integrals for PXZ-XO. There are alternating transfer integrals of 47 and 23 meV for holes and 54 and 35 meV along the directions with the largest charge mobility. In both cases, larger *J* corresponds to the face-to-face π-stacking contact with smaller lateral shift (Figure 5c,d; areas h1 and e1 in Figure 2c). Lower *J* corresponds to the face-to-face packing with large lateral shift and hence weaker orbital overlap; accordingly, green flat areas at the Hirshfeld surface associated with these contacts in Figure 5c,d and 2c (areas h2 and e2) are smaller. The alternation of *J* is lesser than in Crystal 2, and continuous paths of both hole and electron transfer integrals enable reasonable charge mobilities as shown below.

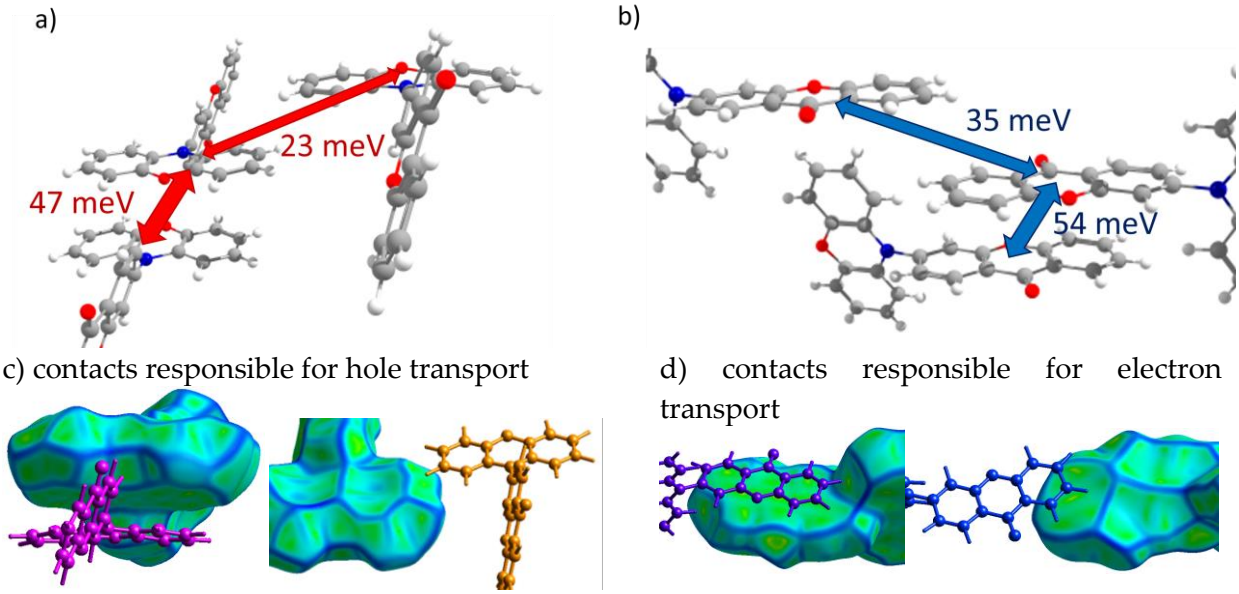

Figure 5. Charge transfer integrals for hole (a) and electron (b) transport in **PXZ-XO**. (c,d) Intermolecular contacts enabling these transfer integrals; left picture corresponds to the contact providing larger *J*, right corresponds to that providing smaller *J*. Hirshfeld surface for central molecule is mapped with curvature C. Coloring corresponds to Figure 2.

TRZ-c-BPXZ (Crystal 4). Transfer integrals for TRZ-BPXZ are shown in **Figure 6a,b**. As follows from it, hole transfer integrals are very small and do not exceed 10 meV. Curiously, they are small even despite of the face-to-face packing of the donor moieties (revealed by large flat green areas in Figure 6c, left, and Figure 2d, area h2) with large orbital overlap in one of the dimers; we attribute this to the phase mismatch of the overlapping HOMOs. As for electrons, considerable J_e are observed for two π-stacking contacts of acceptor (TRZ) moieties (see Figure 6d and Figure 2d, areas e1 and e2). There is a strong alternation of J_e along the stack of the TRZ moieties: one J_e is extremely large and amounts 172 meV, while the other is just 12 meV. This difference is associated with much smaller lateral shifts and hence larger orbital overlap in the former case (more extended contact in Figure 6d, left, larger flat area e1 in Figure 2d).

Preprints (www.preprints.org) | NOT PEER-REVIEWED | Posted: 13 December 2022 doi:10.20944/preprints202212.0225.v1

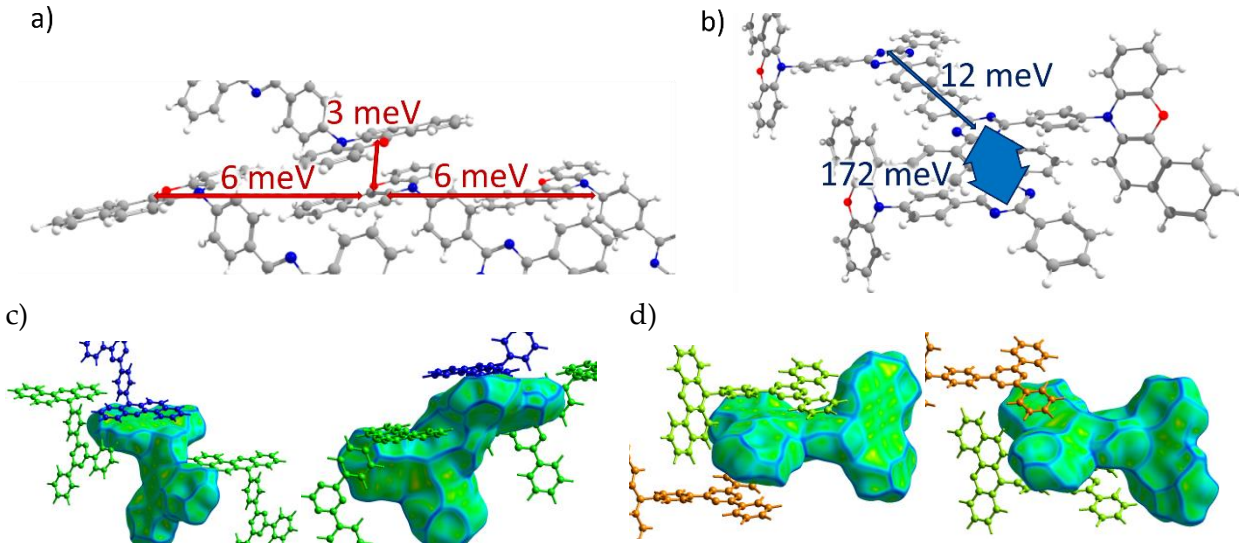

Figure 6. Charge transfer integrals for hole (a) and electron (b) transport in **TRZ-c-BPXZ**. (c,d) Intermolecular contacts enabling these transfer integrals; left picture corresponds to the contact providing larger *J*, right corresponds to that providing smaller *J*. Hirshfeld surface for central molecule is mapped with curvature C. Coloring corresponds to Figure 2

Reorganization energy

Reorganization energies for the compounds studied are presented in Table 2. For oTE-DRZ, they amount to 990 and 440 meV for hole and electron transport, respectively. Huge reorganization energy for hole transfer (cf. ~100 meV for high-mobility OSCs like pentacene and rubrene [32]) can be ascribed to the softness of the donor moiety bearing two sulfur atoms in the central 6-member ring, in line with large λ for TTF derivatives [33, 34], while smaller (but also large) electron reorganization energy can be explained by the higher rigidity and larger size (i.e., better charge delocalization) of the acceptor moiety. For CPPD, hole reorganization is much lower and amounts 220 meV, which can be ascribed to the relatively rigid annulated structure of its donor. In contrast, electron reorganization energy is very large, presumably due to small size and softness of the acceptor (BP) moiety. For PXZ-XO, both hole and electron reorganization energies are moderate due to the annulated nature of donor and acceptor and are comparable to anthracene (~250 meV) that has the same size. For TRZ-c-BPXZ, hole reorganization energy is moderate, which can be also ascribed to the annulated structure of BPXZ moiety. However, electron reorganization energy is very high, which is tentatively assigned to the considerable geometry changes at the bridge between acceptor and donor moieties and triazine ring.

Table 2. Reorganization energies for hole and electron transfer in the crystals studied (in meV).

Compound	*hole*	*electron*
OTE-DRZ (Crystal 1)	990 (540[a])	440 (150[a])
CPPD (Crystal 2)	220	660
PXZ-XO (Crystal 3)	227	255
TRZ-c-BPXZ (Crystal 4)	323	604

[a] Calculated using DFT/HF-3C method.

It is worth noting that the calculated values are upper bound estimates for reorganization energies since they were obtained for isolated molecules, while in the crystal neighboring molecules restrict the geometric relaxation upon charge transfer, especially large-scale relative

Preprints (www.preprints.org) | NOT PEER-REVIEWED | Posted: 13 December 2022 doi:10.20944/preprints202212.0225.v1

rotation of donor and acceptor [13, 33]. To show this, we calculated reorganization energy for oTE-DRZ considering the impact of the crystal environment using ONIOM approach [27]. Specifically, the molecule under investigation was surrounded by the neighboring molecules, and then the calculations necessary for λ estimation (see Section 2) were performed. DFT was applied to the central molecule, while its molecular shell was calculated using composite HF-3C method. In this case, reorganization energy decreases in about twice (see Table 2), which significantly increases charge mobility (Table 3).

Charge mobilities

Table 3 shows the obtained charge carrier mobilities calculated from the J and λ values presented above. As follows from this table, relatively efficient ambipolar transport is predicted for PXZ-XO, with μ_h=0.39 cm^2/(V·s) and μ_e=0.34 cm^2/(V·s). Considerable and comparable mobilities for holes and electrons can be ascribed to comparable and relatively large (~1.5 kT) transfer integrals and moderate reorganization energies. CPPD shows considerable hole mobility mainly due to small λ_h, even although J_h show strong alternation along any direction. On the contrary, electron mobility is one order lower than the hole one due to the large reorganization energy, even despite of large J_e. oTE-DRZ and TRZ-c-BPXZ show low charge mobilities because of the absence of continuous path of transfer integrals or large reorganization energy (for hole transport in oTE-DRZ). Noteworthily, the abovementioned charge mobilities are lower bound estimates since they were obtained using reorganization energies calculated for single molecules without accounting for restriction of the geometry relaxation by the environment. Indeed, considering environment effect on λ using ONIOM approach (see above) can result in considerable increase of charge mobility as shown in Table 3 for oTE-DRZ: for holes, it increases in 8 times reaching 0.016 cm^2/(V·s), while for electrons it increases in about twice reaching 0.156 cm^2/(V·s). Moreover, for oTE-DRZ electron mobility will increase even more (by about twice) if contribution of LUMO+1 is considered.

Table 3. Charge carrier mobilities in the crystals studied.

crystal	*hole mobility*, cm^2/(V·s)	*electron mobility*, cm^2/(V·s)
OTE-DRZ (Crystal 1)	0.002 (0.016*)	0.009 (0.156*)
CPPD (Crystal 2)	0.03	0.002
PXZ-XO (Crystal 3)	0.39	0.34
TRZ-c-BPXZ (Crystal 4)	0.003	0.003

Outlook

Our analysis highlights several structure-property relationships. First, as expected, if donor (acceptor) molecules form continuous π-stacks, considerable hole (electron) mobility can be observed. Noteworthily, in oTE-DRZ, donor and acceptor moieties form segregated stacks, which is favorable for charge transport, probably due to different form of donor and acceptor (planar DRZ and kinked oTE). Tendency for face-to-face packing instead of herringbone packing can be ascribed to non-uniform ESP ((Figure 1) that introduces attractive electrostatic interactions between parallel conjugated cores, in line with Refs. [35-38]. However, in most of the crystals studied donor (acceptor) moieties tend to dimerize, forming tightly bound pairs which weakly

Preprints (www.preprints.org) | NOT PEER-REVIEWED | Posted: 13 December 2022 doi:10.20944/preprints202212.0225.v1

couple to each other. Accordingly, transfer integrals are alternated along the charge transport path, decreasing the mobility. This pairing can stem from the asymmetrical ESP distribution at donor (acceptor) moieties (see Figure 1Fig.), which implies static dipole moment for them and facilitates their antiparallel packing. Finally, both donor and acceptor moieties should be rather rigid to have small reorganization energy, which is important for high charge carrier mobility. As a result, we hypothesize that for efficient charge transport, TADF luminophores should have planar annulated aromatic structure with ESP distribution as symmetrical as possible.

Generally, although the reported charge mobilities above 10^{-3} $cm^2/(Vs)$ are low as compared to high-mobility organic semiconductors, they are appropriate for operation of OLEDs, where charges need to penetrate through thin emission layer (several μm); this is corroborated by reasonable performance of the devices reported in Refs. [6-9]. However, TADF luminophores are also promising for other kinds of light-emitting devices, e.g. organic light-emitting transistors (OLETs) [39]. Using TADF luminophores in non-doped OLETs requires high charge carrier mobilities in the films, since geometry of these devices differs significantly from OLEDs so that charge carriers need to travel much longer distances prior to recombination, and since higher mobilities are required for higher operational frequency. The ambipolar charge carrier mobility of ~0.3 $cm^2/(V·s)$ predicted for PXZ-XO points on the possibility of reaching mobilities at the level of high-mobility crystalline organic semiconductors [32] and amorphous silicon, ~1 $cm^2/(V·s)$.

4. Conclusions

We performed comparative theoretical study of molecular packing and charge transport in four crystals of TADF luminophores. We obtained that among the crystals studied, there is one with considerable mobilities of electrons and holes (~0.3 $cm^2/(V·s)$), in one crystal hole mobility equals ~0.03 cm2/(V·s) and is much larger than the electron one, and in two crystal hole and electron mobilities are comparable and low (less than 0.01 $cm^2/(V·s)$). Expectedly, the largest charge transfer integrals are observed for face-to-face molecular dimers with small lateral shifts; however, the bottleneck is the small transfer integrals between pairs of these tightly interacting dimers in most of the crystals studied. The highest mobility was predicted for compound where donor and acceptor are relatively small condensed heteroaromatics moieties, which enable moderate reorganization energy and moderate alternation of the transfer integrals in the highest-mobility direction. We anticipate that the results obtained will be useful for design of non-doped organic light-emitting diodes, transistors and other light-emitting devices.

Supplementary Materials: The following supporting information can be downloaded at the website of this paper posted on Preprints.org.

Acknowledgements: DFT calculations for single molecules and crystal structure analysis were financially supported by Ministry of Science and Higher Education of the Russian Federation, project FFSM-2022-0004. Charge mobility calculations were performed with the financial support of Russian Science Foundation (project 22-72-10056).

References

1. Huang, Y.; Hsiang, E.-L.; Deng, M.-Y.; Wu, S.-T. Mini-LED, Micro-LED and OLED displays: present status and future perspectives. *Light Sci. Appl.* **2020**, *9*, 105, doi:10.1038/s41377-020-0341-9.
2. Salehi, A.; Fu, X.; Shin, D.-H.; So, F. Recent Advances in OLED Optical Design. *Adv. Funct. Mater.* **2019**, *29*, 1808803, doi:10.1002/adfm.201808803.
3. Lee, S.M.; Kwon, J.H.; Kwon, S.; Choi, K.C. A Review of Flexible OLEDs Toward Highly Durable Unusual Displays. *IEEE Trans Electron Devices* **2017**, *64*, 1922-1931, doi:10.1109/TED.2017.2647964.
4. Hsiang, E.-L.; Yang, Z.; Yang, Q.; Lan, Y.-F.; Wu, S.-T. Prospects and challenges of mini-LED, OLED, and micro-LED displays. *J. Soc. Inf. Disp.* **2021**, *29*, 446-465, doi:10.1002/jsid.1058.
5. Cai, X.; Su, S.-J. Marching Toward Highly Efficient, Pure-Blue, and Stable Thermally Activated Delayed Fluorescent Organic Light-Emitting Diodes. *Adv. Funct. Mater.* **2018**, *28*, 1802558, doi:10.1002/adfm.201802558.
6. Cai, X.; Qiao, Z.; Li, M.; Wu, X.; He, Y.; Jiang, X.; Cao, Y.; Su, S.-J. Purely Organic Crystals Exhibit Bright Thermally Activated Delayed Fluorescence. *Angew. Chem. Int. Ed.* **2019**, *58*, 13522-13531, doi:10.1002/anie.201906371.
7. Gužauskas, M.; Narbutaitis, E.; Volyniuk, D.; Baryshnikov, G.V.; Minaev, B.F.; Ågren, H.; Chao, Y.-C.; Chang, C.-C.; Rutkis, M.; Grazulevicius, J.V. Polymorph acceptor-based triads with photoinduced TADF for UV sensing. *Chem. Eng. J.* **2021**, *425*, 131549, doi:10.1016/j.cej.2021.131549.
8. Zhang, Y.; Ma, H.; Wang, S.; Li, Z.; Ye, K.; Zhang, J.; Liu, Y.; Peng, Q.; Wang, Y. Supramolecular Structure-Dependent Thermally-Activated Delayed Fluorescence (TADF) Properties of Organic Polymorphs. *J. Phys. Chem. C* **2016**, *120*, 19759-19767, doi:10.1021/acs.jpcc.6b05537.
9. Yang, W.; Yang, Y.; Cao, X.; Liu, Y.; Chen, Z.; Huang, Z.; Gong, S.; Yang, C. On-off switchable thermally activated delayed fluorescence controlled by multiple channels: Understanding the mechanism behind distinctive polymorph-dependent optical properties. *Chem. Eng. J.* **2021**, *415*, 128909, doi:10.1016/j.cej.2021.128909.
10. Zhang, Y.; Li, Z.; Li, C.; Wang, Y. Suppressing Efficiency Roll-Off of TADF Based OLEDs by Constructing Emitting Layer With Dual Delayed Fluorescence. *Front. Chem.* **2019**, *7*, 302, doi:10.3389/fchem.2019.00302.
11. Han, J.; Huang, Z.; Miao, J.; Qiu, Y.; Xie, Z.; Yang, C. Narrowband blue emission with insensitivity to the doping concentration from an oxygen-bridged triarylboron-based TADF emitter: nondoped OLEDs with a high external quantum efficiency up to 21.4%. *Chem. Sci.* **2022**, *13*, 3402-3408, doi:10.1039/d2sc00329e.
12. Zhao, G.; Liu, D.; Wang, P.; Huang, X.; Chen, H.; Zhang, Y.; Zhang, D.; Jiang, W.; Sun, Y.; Duan, L. Exceeding 30 % External Quantum Efficiency in Non-doped OLEDs

Utilizing Solution Processable TADF Emitters with High Horizontal Dipole Orientation via Anchoring Strategy. *Angew. Chem. Int. Ed.* **2022**, *61*, e202212861, doi:10.1002/anie.202212861.

13. Danyliv, Y.; Ivaniuk, K.; Danyliv, I.; Bezvikonnyi, O.; Volyniuk, D.; Galyna, S.; Lazauskas, A.; Skhirtladze, L.; Ågren, H.; Stakhira, P.; et al. Carbazole-σ-sulfobenzimide derivative exhibiting mechanochromic thermally activated delayed fluorescence as emitter for flexible OLEDs: Theoretical and experimental insights. *Dyes Pigm.* **2022**, *208*, 110841, doi:10.1016/j.dyepig.2022.110841.
14. Yavuz, I.; Lopez, S.A.; Lin, J.B.; Houk, K.N. Quantitative prediction of morphology and electron transport in crystal and disordered organic semiconductors. *J. Mater. Chem. C* **2016**, *4*, 11238-11243, doi:10.1039/C6TC03823A.
15. Sokolov, A.N.; Atahan-Evrenk, S.; Mondal, R.; Akkerman, H.B.; Sánchez-Carrera, R.S.; Granados-Focil, S.; Schrier, J.; Mannsfeld, S.C.B.; Zoombelt, A.P.; Bao, Z.; et al. From computational discovery to experimental characterization of a high hole mobility organic crystal. *Nat. Commun.* **2011**, *2*, 437, doi:10.1038/ncomms1451.
16. Schober, C.; Reuter, K.; Oberhofer, H. Virtual Screening for High Carrier Mobility in Organic Semiconductors. *J. Phys. Chem. Lett.* **2016**, *7*, 3973-3977, doi:10.1021/acs.jpclett.6b01657.
17. Spackman, P.R.; Turner, M.J.; McKinnon, J.J.; Wolff, S.K.; Grimwood, D.J.; Jayatilaka, D.; Spackman, M.A. CrystalExplorer: a program for Hirshfeld surface analysis, visualization and quantitative analysis of molecular crystals. *J. Appl. Crystallogr.* **2021**, *54*, 1006-1011, doi:10.1107/S1600576721002910.
18. Turner, M.J.; Grabowsky, S.; Jayatilaka, D.; Spackman, M.A. Accurate and Efficient Model Energies for Exploring Intermolecular Interactions in Molecular Crystals. *J. Phys. Chem. Lett.* **2014**, *5*, 4249-4255, doi:10.1021/jz502271c.
19. Mackenzie, C.F.; Spackman, P.R.; Jayatilaka, D.; Spackman, M.A. CrystalExplorer model energies and energy frameworks: extension to metal coordination compounds, organic salts, solvates and open-shell systems. *IUCrJ* **2017**, *4*, 575-587, doi:10.1107/S205225251700848X.
20. Marcus, R.A.; Sutin, N. Electron transfers in chemistry and biology. *Biochim. Biophys. Acta - Bioenerg.* **1985**, *811*, 265-322, doi:10.1016/0304-4173(85)90014-X.
21. Baumeier, B.; Kirkpatrick, J.; Andrienko, D. Density-functional based determination of intermolecular charge transfer properties for large-scale morphologies. *Phys. Chem. Chem. Phys.* **2010**, *12*, 11103-11113, doi:10.1039/C002337J.
22. Kirkpatrick, J. An approximate method for calculating transfer integrals based on the ZINDO Hamiltonian. *Int. J. Quantum Chem* **2008**, *108*, 51-56, doi:10.1002/qua.21378.
23. Kobayashi, H.; Kobayashi, N.; Hosoi, S.; Koshitani, N.; Murakami, D.; Shirasawa, R.; Kudo, Y.; Hobara, D.; Tokita, Y.; Itabashi, M. Hopping and band mobilities of pentacene, rubrene, and 2,7-dioctyl[1]benzothieno[3,2-b][1]benzothiophene (C8-BTBT) from first principle calculations. *J. Chem. Phys.* **2013**, *139*, 014707, doi:10.1063/1.4812389.
24. Coropceanu, V.; Cornil, J.; da Silva Filho, D.A.; Olivier, Y.; Silbey, R.; Brédas, J.-L. Charge Transport in Organic Semiconductors. *Chem. Rev.* **2007**, *107*, 926-952, doi:10.1021/cr050140x.
25. Schmidt, M.W.; Baldridge, K.K.; Boatz, J.A.; Elbert, S.T.; Gordon, M.S.; Jensen, J.H.; Koseki, S.; Matsunaga, N.; Nguyen, K.A.; Su, S.; et al. General atomic and molecular electronic structure system. *J. Comput. Chem.* **1993**, *14*, 1347-1363, doi:10.1002/jcc.540141112.

26. Gordon, M.S.; Schmidt, M.W. Chapter 41 - Advances in electronic structure theory: GAMESS a decade later. In *Theory and Applications of Computational Chemistry*, Dykstra, C.E., Frenking, G., Kim, K.S., Scuseria, G.E., Eds.; Elsevier: Amsterdam, 2005; pp. 1167-1189.
27. Chung, L.W.; Sameera, W.M.C.; Ramozzi, R.; Page, A.J.; Hatanaka, M.; Petrova, G.P.; Harris, T.V.; Li, X.; Ke, Z.; Liu, F.; et al. The ONIOM Method and Its Applications. *Chem. Rev.* **2015**, *115*, 5678-5796, doi:10.1021/cr5004419.
28. Sure, R.; Grimme, S. Corrected small basis set Hartree-Fock method for large systems. *J. Comput. Chem.* **2013**, *34*, 1672-1685, doi:10.1002/jcc.23317.
29. Chemcraft – graphical software for quantum chemical computations, https://www.chemcraftprog.com/
30. Jmol: an open-source Java viewer for chemical structures in 3D. http://www.jmol.org/
31. McKinnon, J.J.; Spackman, M.A.; Mitchell, A.S. Novel tools for visualizing and exploring intermolecular interactions in molecular crystals. *Acta Cryst. B* **2004**, *60*, 627-668, doi:10.1107/S0108768104020300.
32. Ostroverkhova, O. Organic Optoelectronic Materials: Mechanisms and Applications. *Chem. Rev.* **2016**, *116*, 13279-13412, doi:10.1021/acs.chemrev.6b00127.
33. Mas-Torrent, M.; Hadley, P.; Bromley, S.T.; Ribas, X.; Tarrés, J.; Mas, M.; Molins, E.; Veciana, J.; Rovira, C. Correlation between Crystal Structure and Mobility in Organic Field-Effect Transistors Based on Single Crystals of Tetrathiafulvalene Derivatives. *J. Am. Chem. Soc.* **2004**, *126*, 8546-8553, doi:10.1021/ja048342i.
34. Sosorev, A.Y. Simple charge transport model for efficient search of high-mobility organic semiconductor crystals. *Mater. Des.* **2020**, *192*, 108730, doi:10.1016/j.matdes.2020.108730.
35. Watt, M.; Hardebeck, L.K.E.; Kirkpatrick, C.C.; Lewis, M. Face-to-Face Arene−Arene Binding Energies: Dominated by Dispersion but Predicted by Electrostatic and Dispersion/Polarizability Substituent Constants. *J. Am. Chem. Soc.* **2011**, *133*, 3854-3862, doi:10.1021/ja105975a.
36. Trukhanov, V.A.; Dominskiy, D.I.; Parashchuk, O.D.; Feldman, E.V.; Surin, N.M.; Svidchenko, E.A.; Skorotetcky, M.S.; Borshchev, O.V.; Paraschuk, D.Y.; Sosorev, A.Y. Impact of N-substitution on structural, electronic, optical, and vibrational properties of a thiophene–phenylene co-oligomer. *RSC Adv.* **2020**, *10*, 28128-28138, doi:10.1039/D0RA03343J.
37. Sosorev, A.; Dominskiy, D.; Chernyshov, I.; Efremov, R. Tuning of Molecular Electrostatic Potential Enables Efficient Charge Transport in Crystalline Azaacenes: A Computational Study. *Int. J. Mol. Sci.* **2020**, *21*, 5654, doi:10.3390/ijms21165654.
38. Sosorev, A.Y.; Trukhanov, V.A.; Maslennikov, D.R.; Borshchev, O.V.; Polyakov, R.A.; Skorotetcky, M.S.; Surin, N.M.; Kazantsev, M.S.; Dominskiy, D.I.; Tafeenko, V.A.; et al. Fluorinated Thiophene-Phenylene Co-Oligomers for Optoelectronic Devices. *ACS Appl. Mater. Interfaces* **2020**, *12*, 9507-9519, doi:10.1021/acsami.9b20295.
39. Qin, Z.; Gao, H.; Dong, H.; Hu, W. Organic Light-Emitting Transistors Entering a New Development Stage. *Adv. Mater.* **2021**, *33*, 2007149, doi:10.1002/adma.202007149.